

An Information-Geometric Distance on the Space of Tasks

Yansong Gao¹ and Pratik Chaudhari²

¹Applied Mathematics and Computational Science, University of Pennsylvania.

²Department of Electrical and Systems Engineering, University of Pennsylvania.

Email: gaoyans@sas.upenn.edu, pratikac@seas.upenn.edu

Abstract

This paper computes a distance between tasks modeled as joint distributions on data and labels. We develop a stochastic process that transports the marginal on the data of the source task to that of the target task, and simultaneously updates the weights of a classifier initialized on the source task to track this evolving data distribution. The distance between two tasks is defined to be the shortest path on the Riemannian manifold of the conditional distribution of labels given data as the weights evolve. We derive connections of this distance with Rademacher complexity-based generalization bounds; distance between tasks computed using our method can be interpreted as the trajectory in weight space that keeps the generalization gap constant as the task distribution changes from the source to the target. Experiments on image classification datasets show that this task distance helps predict the performance of transfer learning: fine-tuning techniques have an easier time transferring to tasks that are close to each other under our distance.

1 Introduction

A part of the success of Deep Learning stems from the fact that deep networks learn features that are highly discriminative yet flexible. Models pre-trained on a particular task can be easily adapted to perform well on other tasks. The transfer learning literature forms an umbrella for such adaptation techniques. Transfer learning indeed works very well, see for instance [Mahajan et al. \(2018\)](#); [Dhillon et al. \(2020\)](#); [Kolesnikov et al. \(2019\)](#); [Joulin et al. \(2016\)](#) for image classification or [Devlin et al. \(2018\)](#) for language modeling, to name a few of the many large-scale demonstrations. There are however also situations when transfer learning does not work well. For instance, a pre-trained ImageNet model is a poor representation to transfer to images in radiology ([Merkow et al., 2017](#)).

It stands to reason that if source and target tasks are “close” to each other then we should expect transfer learning to work well; it may be difficult to transfer across tasks that are “far away”. We lack theoretical tools that define when two learning tasks are close to each other; while there are numerous candidates in the current literature a unified understanding of these domain-specific methods remains elusive. We also lack algorithmic tools to robustly transfer models on new tasks, for instance, fine-tuning methods require careful design ([Li et al., 2020](#)) and it is unclear what one should do if they do not work well. Our approach on this problem is based on the following two ideas.

Main ideas First, most algorithmic methods that devise a distance between tasks in the current literature, do not take into account the hypothesis space of the model. We argue that transferring the representation of a small model with limited capacity from a source task to a target task is difficult because there are fewer redundant features in the model. The distance between the same two tasks may be small if a high-capacity model is being transferred; this is especially pertinent when transferring deep networks. A definition of task distance or an algorithm for instantiating this definition, therefore needs to take the capacity of the hypothesis class into account.

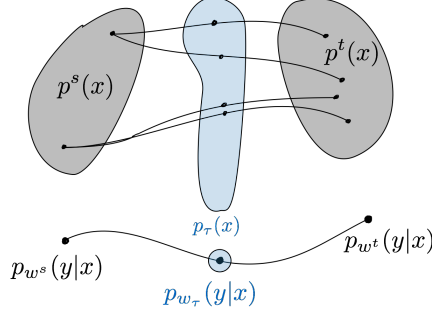


Figure 1: Coupled transfer of the data and the conditional distribution. We solve an optimization problem that transports the source data distribution $p^s(x)$ to the target distribution $p^t(x)$ as $\tau \rightarrow 1$ while simultaneously updating the model using samples from the interpolated distribution $p_\tau(x)$. This modifies the conditional distribution $p_{w^s}(y|x)$ on the source task to the corresponding distribution on the target task $p_{w^t}(y|x)$. Distance between source and target tasks is defined to be the length of the optimal trajectory of the weights under the Fisher Information Metric.

Second, distance between tasks as measured using techniques in the current literature does not take into account the dynamics of learning; distances often depend on how the transfer was performed. For instance, if one considers the number of epochs of fine-tuning required to reach a certain accuracy, a different strategy may result in a different distance. A sound notion of distance between tasks should not depend on the specific dynamical process used of transfer.

Summary of contributions Given data x and labels y , we model the source and target tasks as joint distributions $p^s(x, y)$ and $p^t(x, y)$ respectively where

$$p^s(x, y) = p_{w^s}^s(y|x) p^s(x);$$

here w^s are the parameters (weights) of a classifier on the source task. The target task is decomposed analogously. We define the distance between finite-sample *datasets* $\hat{p}^s = \{(x_i, y_i) \sim p^s\}_{i=1}^{N_s}$ drawn from tasks (with \hat{p}^t defined analogously) as the solution of the optimization problem

$$\begin{aligned} \min_{\Gamma \in \Pi} \int_0^1 \mathbb{E}_{(x,y) \sim p_\tau(x,y)} \left[\sqrt{2\text{KL}(p_{w_\tau}(\cdot|x), p_{w_{\tau+d\tau}}(\cdot|x))} \right] \\ \text{subject to } \frac{dw_\tau}{d\tau} = \hat{\nabla}_w \left\{ \mathbb{E}_{(x,y) \sim p_\tau} [\log p_{w_\tau}(y|x)] \right\}; \end{aligned} \quad (1)$$

where

$$\begin{aligned} p_\tau(x, y) &= \sum_{i=1}^{N_s} \sum_{j=1}^{N_t} \Gamma_{ij} \delta_{\{(1-\tau)x_i^s + \tau x_j^t\}} \delta_{\{(1-\tau)y_i^s + \tau y_j^t\}}, \\ \Pi &= \left\{ \Gamma \in \mathbb{R}_+^{N_s \times N_t} : \Gamma \mathbf{1} = \hat{p}^s, \Gamma^\top \mathbf{1} = \hat{p}^t \right\}. \end{aligned} \quad (2)$$

The square root of the KL-divergence measures the infinitesimal distance traveled along a geodesic on the manifold of probability distributions $p_{w_\tau}(y|x)$. Distance as defined in (1) and (2) is the path length on this manifold. Weights $w(\tau)$ evolve from their initial value w^s using stochastic gradient descent-based updates in (1) while the interpolated data distributed p_τ to which weights are being fitted to evolves simultaneously from its initial value p^s to its final value p^t using the linear coupling matrix Γ .

The distance in (1) is the Fisher-Rao distance on the manifold of distributions $p_w(y|x)$. We use this to draw a link to Rademacher complexity-based generalization bounds which gives an intuitive understanding of

the trajectory of weights computed in (1). We show that our approach modifies the task’s data distribution and weights so as to minimize the *average generalization gap* along the trajectory that joins the weights on the source task w^s to their terminal value on the target task $w(1)$.

We devise an algorithmic procedure to solve the optimization problem in (1) and (2) for image classification tasks that are subsets of CIFAR-10 and CIFAR-100 datasets (Krizhevsky and Hinton, 2009). We show in Sec. 4 that the coupled transfer process estimates distances that are more consistent with the difficulty of fine-tuning, as compared to baselines.

2 Theoretical setup

Consider a dataset $\widehat{p}^s = \{(x_i, y_i) \sim p^s\}_{i=1, \dots, N_s}$ where $x_i \in X, y_i \in Y$ denote input data and their ground-truth annotations respectively. Data are drawn from a distribution p^s supported on $X \times Y$. Training a parameterized model, say a deep network, involves minimizing the cross-entropy loss $\ell^s(w) := -\frac{1}{N_s} \sum_{i=1}^{N_s} \log p_w(y_i|x_i)$ using a sequence of weight updates

$$\frac{dw(\tau)}{d\tau} = -\widehat{\nabla} \ell^s(w); w(0) = w^s; \quad (3)$$

these are typically implemented using Stochastic Gradient Descent (SGD). The notation $\widehat{\nabla} \ell^s(w)$ indicates a stochastic estimate of the gradient using a subset of the data.

We will denote the marginal of the joint distributions on the input data as $p^s(x)$ and $p^t(x)$ respectively.

2.1 Low-capacity models are difficult to transfer

The Information Bottleneck (IB) Principle (Tishby et al., 2000) abstracts a parametric classifier as a Markov chain $x \rightarrow z \rightarrow y$ where z is called the representation. The main idea behind IB is to learn sufficient and minimal representations that discard information in the data that are not relevant to predicting labels (Shwartz-Ziv and Tishby, 2017). Gao and Chaudhari (2020) build upon this idea to design a Lagrangian to study transfer learning

$$F_{p^s}(\lambda, \gamma) = \min_{e(z|x), d(x|z), c(y|z)} \{R + \lambda D + \gamma C\}. \quad (4)$$

Here $e(z|x)$ is an encoder that constructs the representation z , $c(y|z)$ predicts the labels and $d(x|z)$ is the decoder measures the trade-off between redundant features that give a lossless representation of the data and discriminative features for the classifier. The quantities R, D and C are the rate of the encoder, distortion of the decoder and the classification loss respectively (see Sec. A for more details).

The situation with a low-capacity model (encoder and classifier) can be modeled as follows. If source and target task are similar then transfer is easy because features of the encoder trained on source are also good for the target. If the tasks are dissimilar, observe that KKT conditions give $dF_{p^s} = -dR - \lambda dD - \gamma dC$. A low-capacity model needs a large γ to achieve the same classification loss C which according to the KKT condition leads to larger value of the D (for fixed λ). This indicates that the model does not learn redundant features that may be potentially useful on a dissimilar target task. This is not the case for a model with large capacity where (4) learns both redundant and discriminative features, without being forced to make a trade-off between them.

2.2 Fisher-Rao metric on the manifold of probability distributions

Consider a manifold $M = \{p_w(z) : w \in \mathbb{R}^p\}$ of probability distributions. Information Geometry (Amari, 2016) studies invariant geometrical structures on such manifolds. For two points $w, w' \in M$, we can use the Kullback-Leibler (KL) divergence $\text{KL}[p_w, p_{w'}] = \int dp_w(z) \log(p_w(z)/p_{w'}(z))$, to obtain a Riemannian

structure on M . Such a structure allows the infinitesimal distance ds on the manifold to be written as

$$ds^2 = 2\text{KL}[p_w, p_{w+dw}] = \sum_{i,j=1}^p g_{ij} dw_i dw_j \quad (5)$$

where the Fisher Information Matrix (FIM) (g_{ij}) with each

$$g_{ij}(w) = \int dp_w(z) (\partial_{w_i} \log p_w(z)) (\partial_{w_j} \log p_w(z)) \quad (6)$$

is positive-definite. The weights w play the role of a coordinate system for computing the distance. The FIM is the Hessian of the KL-divergence; we may think of the FIM as quantifying the amount of information present in the model about the data it was trained on. The FIM is the unique metric on M (up to scaling) that is preserved under diffeomorphisms (Bauer et al., 2016). This property motivated Liang et al. (2019) to define a geometric notion of model complexity called the Fisher-Rao norm as

$$\|w\|_{\text{fr}}^2 = \langle w, g w \rangle. \quad (7)$$

This will be discussed further in Sec. 3.3.

Given a continuously differentiable curve $\{w(\tau)\}_{\tau \in [0,1]}$ on the manifold M we can compute its length by integrating the infinitesimal distance $|ds|$ along it. The shortest length curve between two points $w, w' \in M$ induces a metric on M known as the Fisher-Rao distance (Rao, 1945)

$$d_{\text{FR}}(w, w') = \min_{\substack{w: w(0)=w \\ w(1)=w'}} \int_0^1 \sqrt{\langle \dot{w}(\tau), g(w(\tau)) \dot{w}(\tau) \rangle} d\tau; \quad (8)$$

Let us note that shortest paths on a Riemannian manifold are geodesics, i.e., they are locally “straight lines”.

Assumption 1 (Fisher-Rao distance is computed only for the conditional distribution). Although we are interested in the manifold of joint distributions we will only parametrize the conditional, i.e., we write

$$p_w^s(x, y) := p^s(x) p_w(y|x). \quad (9)$$

The marginal on input is not parameterized. This is a simplifying assumption and allows us to decouple the data distribution from the conditional; we can tackle the former using techniques in optimal transport and the latter using techniques in information geometry. Parameterizing the joint distribution directly and using a unified approach to compute the task distance is possible but will require generative modeling of $p^s(x)$ which is computationally challenging.

Under Assumption 1, the FIM in (6) can be written as

$$g_{ij}(w) = \mathbb{E}_{x \sim p^s(x), y \sim p_w(y|x)} [\partial_{w_i} \log p_w(y|x) \partial_{w_j} \log p_w(y|x)].$$

The FIM is difficult to compute for large models and approximations often work poorly (Kunstner et al., 2019). Notice that we do not need to compute the FIM but only need to compute the distance $|ds|$. Given a trajectory of weights $\{w(\tau)\}_{\tau \in [0,1]}$ we can compute its length directly by averaging the square root of the KL-divergence between the conditional distributions of labels given data.

2.3 Transporting the data distribution

We next focus on the marginals on the input data. We would like to modify the input distribution from $p^s(x)$ to $p^t(x)$ during transfer. We will use tools from optimal transportation (OT) for this purpose; see Santambrogio (2015); Peyré and Cuturi (2019) for an elaborate introduction to OT.

Let $\Pi(p^s, p^t)$ be the set of joint distributions with first marginal equal to $p^s(x)$ and second marginal $p^t(x')$. The Kantorovich relaxation of the OT problem solves for

$$W_2^2(p^s, p^t) = \inf \left\{ \int \|x - x'\|^2 d\gamma : \gamma \in \Pi(p^s, p^t) \right\}$$

to compute the best joint coupling $\gamma^* \in \Pi$. The solution of this problem is the Wasserstein metric $W_2(p^s, p^t)$ between the two distributions. In this paper, we are interested, not in the Wasserstein metric, but the transport trajectory that the optimal coupling γ^* entails. This is the subject of displacement interpolation (McCann, 1997): it turns out that the geodesic that joins p^s and p^t is a locally distance minimizing curve in the W_2 metric. If p_τ is the distribution at an intermediate step $\tau \in [0, 1]$, we have

$$W_2(p^s, p_\tau) = \tau W_2(p^s, p^t).$$

The path that the optimal coupling γ^* takes is therefore a *constant-speed* geodesic.

We are interested in instantiating this idea for source and target input *datasets* (we denote these by $\hat{p}^s(x)$ and $\hat{p}^t(x)$) that consist of finite samples N_s and N_t respectively. The development is more convenient in this case and the set of transport plans is a (convex) polytope

$$\Pi(\hat{p}^s, \hat{p}^t) = \left\{ \Gamma \in \mathbb{R}_+^{N_s \times N_t} : \Gamma \mathbb{1}_{N_s} = \hat{p}^s, \Gamma^\top \mathbb{1}_{N_t} = \hat{p}^t \right\} \quad (10)$$

and the optimal coupling is given by

$$\Gamma^* = \underset{\Gamma \in \Pi(\hat{p}^s, \hat{p}^t)}{\operatorname{argmin}} \{ \langle \Gamma, C \rangle - \epsilon H(\Gamma) \} \quad (11)$$

where $C_{ij} = \|x_i - x'_j\|_2^2$ is the matrix of pairwise distances between the source and target data. The inner product in the first term measures the total cost $\sum_{ij} \Gamma_{ij} C_{ij}$ incurred for the transport and minimizing it directly is typically done using interior point methods. This can be accelerated using an entropic penalty $H(\Gamma) = -\sum_{ij} \Gamma_{ij} \log \Gamma_{ij}$ popularized by Cuturi (2013). McCann’s interpolation for the finite-dimensional case with the quadratic loss C_{ij} can be written explicitly as the distribution

$$p_\tau(x) = \sum_{i=1}^{N_s} \sum_{j=1}^{N_t} \Gamma_{ij}^* \delta_{(1-\tau)x_i + \tau x'_j}(x). \quad (12)$$

Notice that this is a sum of Dirac-delta distributions supported at interpolated *input data* $x = (1 - \tau)x_i + \tau x'_j$. We can also create pseudo labels for samples from p_τ by a linear interpolation of the one-hot encoding of their respective labels to get

$$p_\tau(x, y) = \sum_{i=1}^{N_s} \sum_{j=1}^{N_t} \Gamma_{ij}^* \delta_{(1-\tau)x_i + \tau x'_j}(x) \delta_{(1-\tau)y_i + \tau y'_j}(y). \quad (13)$$

Modifications to the interpolated distribution We next make two practically motivated modifications to the interpolated distribution $p_\tau(x, y)$.

First, the quadratic distance $C_{ij} = \|x_i - x'_j\|_2^2$ is not a reasonable notion of visual/text data that have strong local correlations. It is therefore beneficial to compute C_{ij} using a feature extractor, say a large neural network φ , that is trained on some generic task

$$C_{ij} := \|\varphi(x_i) - \varphi(x'_j)\|_2^2. \quad (14)$$

This gives us a good coupling matrix Γ in practice because the feature space $\varphi(x)$ is much more Euclidean-like than the original input space; similar ideas are often employed in the metric learning literature (Snell et al., 2017; Hu et al., 2015; Qi et al., 2018).

Second, the peculiar form of the interpolating distribution in (13) that consists of convex combinations of inputs and labels is the result of the quadratic cost. Samples from such an interpolated distribution will have visual artifacts for image-based data. In practice, we treat the time τ as parameter of a Beta-distribution $\text{Beta}(\tau, 1 - \tau)$. Thereby samples from p_τ are similar to those created in Mixup regularization Zhang et al. (2017); a fraction τ of the samples are similar to those from p^s and the remainder are similar to those from p^t . Note that which data is used to form the Mixup combinations is still governed by the coupling matrix Γ^* . We use this trick for both inputs and labels in our experiments.

3 Methods

We now combine the development of Sec. 2.2–2.3 to transport the marginal on the data and modify the weights on the statistical manifold. This section also discusses techniques to efficiently implement the approach and make it scalable to large deep networks. Sec. 3.3 discusses an alternate perspective on this coupled transfer process using the connection between Rademacher complexity and the Fisher-Rao norm.

3.1 Interpolating tasks using a mixture distribution

Interpolating the source and target tasks using a mixture distribution is a simple way to demonstrate the main idea of our approach. For $\tau \in [0, 1]$, consider

$$p_\tau(x, y) = (1 - \tau)p^s(x, y) + \tau p^t(x, y). \quad (15)$$

This amounts to, on average, $1 - \tau$ fraction of samples from \hat{p}^s and the rest from \hat{p}^t . At time instant τ , weights of the classifier are updated using SGD to fit samples from p_τ . We write this as

$$\frac{dw_\tau}{d\tau} = \hat{\nabla}_w \mathbb{E}_{(x,y) \sim p_\tau} [\log p_{w_\tau}(y|x)]; \quad w(0) = w^s \quad (16)$$

Weights w_τ can be thought of as fitted to the task p_τ for every τ , in particular for $\tau = 1$, the weights $w(1)$ is fitted to p^t . We can now integrate the length of the trajectory using (8) to compute the distance between tasks.

Changes in the data distribution and updates to the weights are not synchronized in this approach. For instance, changes in the data may be unfavorable to the current weights and this forces a different trajectory in the weight space as the weights struggle to track p_τ . If changes in data were synchronized with those in weights, the weight trajectory would be different *and necessarily shorter* because the KL-divergence in (5) is large if the conditional distribution changes quickly; our experimental results also corroborate this.

3.2 Modifying the task and weights simultaneously

We now reintroduce the transport process for the data distribution. For a coupling matrix Γ , the interpolated distribution corresponding to the squared Euclidean cost in OT is given by (13). Observe that since $\Gamma \in \mathbb{R}^{N_s \times N_t}$, the (ij) th entry of this matrix indicates the interpolation of source input $x_i^s \in \hat{p}^s$ with that of target input $x_j^t \in \hat{p}^t$. The distance between two tasks as defined in (1) and (2) can now be computed for the two datasets \hat{p}^s and \hat{p}^t iteratively as follows. Given an initialization Γ^0 computed using a feature extractor in (14),

we perform the following updates at each iteration.

$$\Gamma^{k+1} = \underset{\Gamma \in \Pi}{\operatorname{argmin}} \left\{ \langle \Gamma, C^k \rangle - \epsilon H(\Gamma) - \lambda^{-1} \langle \Gamma, \Gamma^k \rangle \right\}, \quad (17a)$$

$$C_{ij}^k = \int_0^1 \sqrt{2\operatorname{KL} \left[p_{w_\tau^k}(\cdot | x_{ij}^\tau), p_{w_{\tau+d\tau}^k}(\cdot | x_{ij}^\tau) \right]}, \quad (17b)$$

$$\frac{dw_\tau^{k+1}}{d\tau} = \widehat{\nabla}_w \left\{ \mathbb{E}_{(x,y) \sim p_\tau} \left[\log p_{w_\tau^{k+1}}(y|x) \right] \right\}, \quad (17c)$$

$$p_\tau(x, y) = \sum_{i=1}^{N_s} \sum_{j=1}^{N_t} \Gamma_{ij}^k \delta_{(1-\tau)x_i^s + \tau x_j^t}(x) \delta_{(1-\tau)y_i^s + \tau y_j^t}(y). \quad (17d)$$

At each iteration, the matrix of costs C_{ij}^k is used to store the cost of transporting the input x_i^s to x_j^t along the weight trajectory $\{w_\tau^k\}_{\tau \in [0,1]}$ obtained in (17c); all trajectories are initialized at $w^k(0) = w^s$. Observe that the transport cost has the length of the trajectory in weight space (the integral in (8)) incorporated into it. This is our current candidate for the OT cost matrix, similar to one in (11). Given these costs, we can compute the new coupling matrix Γ^{k+1} using (17a) which is in turn used in the next iteration to compute the interpolated distribution p_τ via (17d). Computing the task distance is a non-convex optimization problem and we therefore include a proximal term in (17a) to keep the coupling matrix close to the one in the previous step Γ^k . This has the added effect of keeping the entire trajectory of weights $\{w_\tau^{k+1}\}_{\tau \in [0,1]}$ close to the trajectory in the previous iteration. Proximal point iteration (Bauschke and Combettes, 2017) is insensitive to the step-size λ and it is therefore beneficial to employ it in these updates.

Let us note that the task distance computed in (17) is asymmetric, the length of the trajectory for transferring from \widehat{p}^s to \widehat{p}^t is different from the one that transfers from \widehat{p}^t to \widehat{p}^s .

Remark 2 (Fisher-Rao distance can be compared across different architectures). The length of the shortest path between two points on the manifold of distributions $p_w(y|x)$, namely the Fisher-Rao distance, does not depend on the embedding dimension of the manifold M . More specifically, the distance between tasks as computed by this length does not depend on the number of parameters of the neural architecture, it only depends upon the capacity to fit the conditional distribution $p_w(y|x)$. This enables a desirable property: for the same two tasks, task distance using our approach is numerically comparable across different architectures.

Remark 3 (Scaling up the computation). The formulation in (17) updates $\Gamma \in \mathbb{R}^{N_s \times N_t}$ and $w_\tau \in \mathbb{R}^p$. Executing the updates, even for large deep networks and standard datasets is easy for the weights. The coupling matrix Γ has a large number of entries and it is therefore challenging. Some common approaches to handling large-scale OT problems are hierarchical methods (Lee et al., 2019), and greedy computation (Carlier et al., 2010). In practice, we initialize (17a) with a block-diagonal approximation of the coupling matrix using (14) as the costs and perform mini-batch updates on the non-zero entries of Γ . At each iteration, we sample from the interpolated distribution (17d) using only entries of Γ^k that are a part of the mini-batch. Experiments in Sec. 4 show that the weight trajectory converges under such mini-batch updates of Γ^k .

3.3 An alternative perspective via Rademacher complexity

We next study how the trajectory given by the formulation of (17) looks under the lens of learning theory. We show that we can interpret the solution of coupled transfer as a trajectory that minimizes the integral of the generalization gap as the task and the weights are modified. This gives us an intuitive understanding of what qualifies as good transfer; indeed weight trajectories that do not lead to degradation of the generalization gap result in weights on the target task w^t that also generalize well.

We introduce a few quantities before giving the main result. We consider binary classification in this section for clarity. Given a $w \in A$, we define the empirical Rademacher complexity (Bartlett and Mendelson, 2001) as

$$\widehat{\mathcal{R}}_N(A) = \mathbb{E}_\sigma \left[\sup_{w \in A} \frac{1}{N} \sum_{i=1}^N \epsilon^i \ell(w; x^i, y^i) \right], \quad (18)$$

where σ^i are independent and uniformly distributed on $\{-1, 1\}$ and $\ell(w; x^i, y^i)$ is the loss on the i^{th} datum of a dataset \hat{p} with N samples. We will choose the set A to be the r -ball in the Fisher-Rao norm

$$A := \{w : \|w\|_{\text{fr}} \leq r\},$$

and write the corresponding complexity as $\hat{\mathcal{R}}_N(r)$. The Rademacher complexity is the expectation of the empirical complexity over draws of different datasets

$$\mathcal{R}_N(r) = \mathbb{E}_{\hat{p} \sim p} \left[\hat{\mathcal{R}}_N(r) \right].$$

The classical Rademacher complexity-based generalization bound characterizes the ability of binary classifiers h in a hypothesis class $h \in \mathcal{H}$ to fit random noise. We have that for all $h \in \mathcal{H}$ the absolute value of the generalization error and the training error is upper bounded by

$$\mathcal{R}_{2N}(\mathcal{H}) + 2\sqrt{\frac{\log(1/\delta)}{N}} \quad (19)$$

with probability at least $1 - \delta$. We build upon this to obtain the following theorem.

Theorem 4. Given a trajectory of the weights $\{w_\tau\}_{\tau \in [0,1]}$ and a sequence $0 \leq \tau_1 < \tau_2 < \dots < \tau_K \leq 1$, then for all $\epsilon > \frac{2}{K} \sum_{k=1}^K \mathcal{R}_N(\|w_{t_k}\|_{\text{fr}})$, the probability that

$$\frac{1}{K} \sum_{k=1}^K \left(\mathbb{E}_{(x,y) \sim p_{\tau_k}} [\ell(w_{\tau_k}, x, y)] - \frac{1}{N} \sum_{(x,y) \sim \hat{p}_{\tau_k}} \ell(w_{\tau_k}, x, y) \right)$$

is greater than ϵ is upper bounded by

$$\exp \left\{ -\frac{2K}{M^2} \left(\epsilon - \frac{2}{K} \sum_{k=1}^K \mathcal{R}_N(\|w_{t_k}\|_{\text{fr}}) \right)^2 \right\}. \quad (20)$$

The proof is provided in Sec. D. In other words, ensuring that the generalization gap of the model is small during transfer can be achieved by ensuring that the Rademacher complexity $\mathcal{R}_N(\|w_\tau\|_{\text{fr}})$ is small at all times during transfer.

Specializing the result for multi-layer linear models. Characterizing the Rademacher complexity of the r -ball in Fisher-Rao norm is difficult. However, for multi-layer linear classifiers with input domain $X \subset \mathbb{R}^p$, [Liang et al. \(2019\)](#) showed that

$$\mathcal{R}_N(r) \leq r \sqrt{\frac{p}{N}}$$

assuming the data covariance matrix $\mathbb{E}_{x \sim p}[x^\top x]$ is full-rank. For such a model, minimizing the integral of the Rademacher complexity is achieved by minimizing

$$\int_0^1 \sqrt{\langle w_\tau, g(w_\tau) w_\tau \rangle} d\tau; \quad (21)$$

which is an upper-bound on the Fisher-Rao distance of the trajectory between p_{w^s} and p_{w^t} . The optimization problem in (17) finds the latter and we have thus obtained a close connection between the coupled transfer process and the intuitive idea that as the model is transferred, keeping the generalization gap small at all instants of the trajectory would lead to a good generalization gap on the target dataset.

As the authors in [Liang et al. \(2019\)](#) discuss further, the Fisher-Rao norm ball is an envelope of popular norms such as spectral norm ([Bartlett et al., 2017](#)), group norm ([Neyshabur et al., 2015b](#)) and path norm ([Neyshabur et al., 2015a](#)) introduced to characterize the complexity of deep neural networks. The Rademacher complexity using these other norms can therefore be upper-bounded in terms of the Fisher-Rao norm, which leads to a similar conclusion for non-linear models.

3.3.1 A refined result on the connection between the Fisher-Rao distance on the manifold and generalization error on the interpolating distribution

The upper bound in Thm. 4 states that we should minimize the Rademacher complexity of the hypothesis space in order to ensure that the weight trajectory has a small generalization gap at all time instants. For linear models, the Rademacher complexity can be related to the Fisher-Rao norm $\langle w, gw \rangle$. The Fisher-Rao distance on the manifold, namely

$$\int_0^1 \mathbb{E}_{x \sim p_\tau(x)} \left[\sqrt{2\text{KL}(p_{w_\tau}(\cdot|x), p_{w_{\tau+d\tau}}(\cdot|x))} \right] d\tau = \int_0^1 \mathbb{E}_{x \sim p_\tau(x)} \sqrt{\langle \dot{w}_\tau, g(w_\tau) \dot{w}_\tau \rangle} d\tau$$

is only a lower bound on the integral of the Fisher-Rao norm along the weight trajectory. We therefore make some additional assumptions in this section to draw out a crisp link between the Fisher-Rao *distance* and the generalization gap along the trajectory.

Theorem 5. Given a trajectory of the weights $\{w_\tau\}_{\tau \in [0,1]}$ and a sequence $0 = \tau_0 \leq \tau_1 < \tau_2 < \dots < \tau_K \leq 1$, for all $\epsilon > 2 \sum_{k=1}^K (\tau_k - \tau_{k-1}) \mathbb{E}_{x \sim p_\tau} |\Delta \ell(w_{\tau_{k-1}})|$, the probability that

$$\frac{1}{K} \sum_{k=1}^K \left(\mathbb{E}_{(x,y) \sim p_{\tau_k}} [\ell(w_{\tau_k}, x, y)] - \frac{1}{N} \sum_{(x,y) \sim \hat{p}_{\tau_k}} \ell(w_{\tau_k}, x, y) \right)$$

is greater than ϵ is upper bounded by

$$\exp \left\{ -\frac{2K}{M^2} \left(\epsilon - 2 \sum_{k=1}^K (\tau_k - \tau_{k-1}) \mathbb{E}_{x \sim p_{\tau_k}} [|\Delta \ell(w_{\tau_{k-1}})|] \right) \right\}. \quad (22)$$

We have defined the shorthand $\Delta \ell(w_\tau) := \ell(w_{\tau+d\tau}; x, y_\tau(x)) - \ell(w_\tau; x, y_\tau(x))$.

Proof is provided in Sec. E. This shows that computing the Fisher-Rao distance between two points on the statistical manifold results in a weight trajectory that minimizes the the generalization gap of weights trained on the interpolated distribution along the trajectory. In other words, one may either think of our coupled transfer process as computing the Fisher-Rao distance or as finding a weight trajectory that connects weights with a small generalization gap.

4 Experimental evidence

This section discusses experiments on image classification datasets which demonstrate that the distance computed using our methods is consistent with the difficulty of fine-tuning from the source dataset to the target dataset. We compare and contrast our distance estimates with existing methods, discuss how the optimization problem in (17) converges to its solution across iterations and show that larger models are easier to transfer between tasks.

4.1 Setup

We use the CIFAR-10, CIFAR-100 datasets for our experiments. Source and target tasks consist of subsets of these datasets, each task with one or more of the original classes inside it. We show results using an 8-layer convolutional neural network with ReLU nonlinearities, dropout, batch-normalization with a final fully-connected layer along with a larger wide-residual-network (WRN-16-4, (Zagoruyko and Komodakis, 2016)). More details of pre-processing, architecture and training procedure are provided in Sec. B.

Baselines The first baseline is Task2Vec (Achille et al., 2019a) which embeds tasks using the diagonal of the FIM of a model trained on them individually; cosine distance between these vectors is defined as the distance. We compute the robust approximation of the FIM via Monte Carlo updates as done by the original authors.

The second baseline (fine-tuning) directly computes the length of the trajectory in the weight space, i.e., $\int |dw|$. The trajectory is truncated when validation accuracy on the target task is 95% of its final validation accuracy. Note that no adaptation of input data is performed and the model directly takes SGD updates on the target task after being pre-trained on the source task. The learning rate for each model was tuned across all datasets to ensure that the validation accuracy on the target dataset is good and fixed thenceforth for all experiments. The number of epochs required for fine-tuning is a popular way to measure distance between tasks (Kornblith et al., 2019).

The third baseline (uncoupled transfer) uses a mixture of the source and target data, where the interpolating parameter is sampled from $\text{Beta}(\tau, 1 - \tau)$ (see Sec. 3.1) in order to be consistent with the way we implement coupled transfer and avoid visual artifacts in the input data. Length of the trajectory is computed using the FIM metric in this case, which enables direct comparison of the task distances for coupled and uncoupled transfer.

4.2 Transferring between CIFAR-10 and CIFAR-100

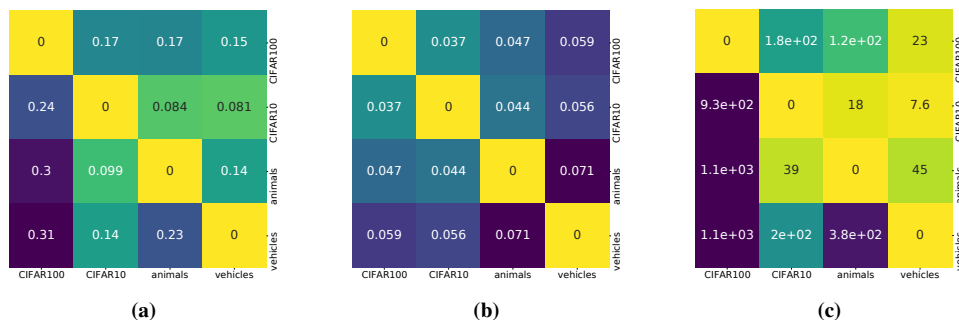


Figure 2: Fig. 2a shows distances (numbers in the cell) computed using our coupled transfer process, Fig. 2b shows distances estimated using Task2Vec while Fig. 2c shows the distance estimating using fine-tuning. The numerical values of the distances in this figure are not comparable with each other. Coupled transfer distances satisfy certain sanity checks, e.g., transferring to a subset task is easier than transferring from a subset task (CIFAR-10-vehicles/animals).

We consider four tasks (i) all vehicles (airplane, automobile, ship, truck) in CIFAR-10, (ii) the remainder, namely six animals in CIFAR-10, (iii) the entire CIFAR-10 dataset and (iv) the entire CIFAR-100 dataset. We show results in Fig. 2 using 4×4 distance matrices where numbers in each cell indicate the distance between the source task (row) and the target task (column).

Coupled transfer shows similar trends as fine-tuning, e.g., the tasks animals-CIFAR-10 or vehicles-CIFAR-10 are close to each other while CIFAR-100 is far away from all tasks (it is closer to CIFAR-10 than others). Task distance is asymmetric in Fig. 2a, Fig. 2c. Distance from CIFAR-10-animals is smaller than animals-CIFAR-10; this is expected because animals is a subset of CIFAR-10. Task2Vec distance estimates in Fig. 2b are qualitatively quite different from these two; the distance matrix is symmetric. Also, while fine-tuning from animals-vehicles is relatively easy, Task2Vec estimates the distance between them to be the largest.

This experiment also shows that our approach can scale to medium-scale datasets and can handle situations when the source and target task have different number of classes.

4.3 Transferring among subsets of CIFAR-100

We construct five tasks (herbivores, carnivores, vehicles-1, vehicles-2 and flowers) that are subsets of the CIFAR-100 dataset. Each of these tasks consists of 5 sub-classes. The distance matrices for coupled transfer,

Task2Vec and fine-tuning are shown in Fig. 3a, Fig. 3b and Fig. 3c respectively. We also show results using uncoupled transfer in Fig. 3d.

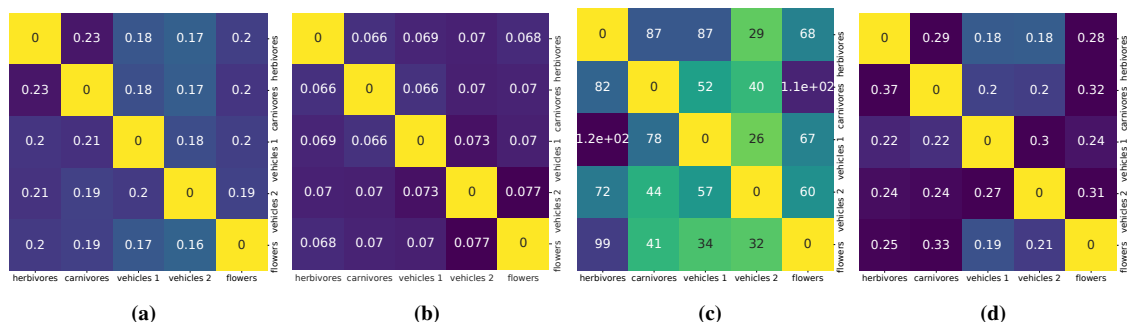


Figure 3: Fig. 3a shows the distance for coupled transfer, Fig. 3b shows the distance for Task2Vec, Fig. 3c shows the distance for fine-tuning and Fig. 3d shows the distance for uncoupled transfer. Numerical values the first and the last sub-plot can be compared directly. Coupled transfer broadly agrees with fine-tuning except for carnivores-flowers and herbivores-vehicles-1. For all tasks, uncoupled transfer overestimates the distances compared to Fig. 3a.

Coupled transfer estimates that all these subsets of CIFAR-100 are roughly equally far away from each other with herbivores-carnivores being the farthest apart while vehicles-1-vehicles-2 being closest. This ordering is consistent with the fine-tuning distance although fine-tuning results in an extremely large value for carnivores-flowers and vehicles-1-herbivores. This ordering is mildly inconsistent with the distances reported by Task2Vec in Fig. 3b the distance for vehicles-1-vehicles-2 is the highest here. Broadly, Task2Vec also results in a distance matrix that suggests that all tasks are equally far away from each other. As has been reported before (Li et al., 2020), this experiment also demonstrates the fragility of fine-tuning.

Recall that distances for uncoupled transfer in Fig. 3d can be comparable directly to those in Fig. 3a for coupled transfer. Task distances for the former are always larger. Further, distance estimates of uncoupled transfer do not bear much resemblance with those of fine-tuning; see for example the distances for vehicles-2-carnivores, flowers-carnivores, and vehicles-1-vehicles-2. This demonstrates the utility of solving a coupled optimization problem in (17) which finds a shorter trajectory on the statistical manifold.

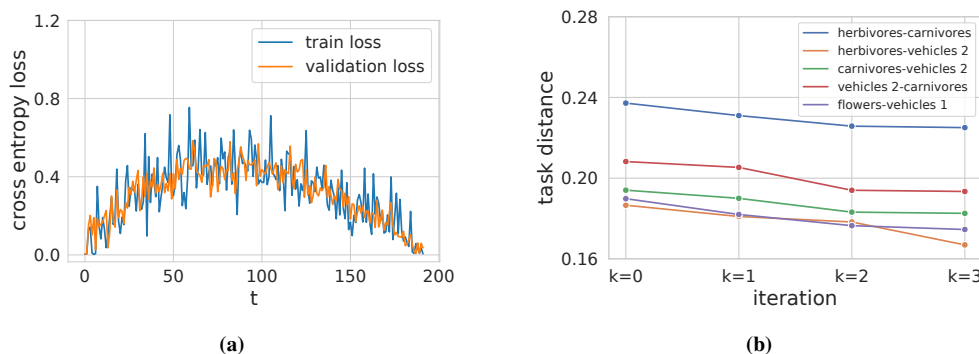


Figure 4: Fig. 4a shows the evolution of the training and test cross-entropy loss on the interpolated distribution as a function of the transfer steps in the final iteration of coupled transfer of vehicles-1-vehicles-2. As predicted by Thm. 4, generalization gap along the trajectory is small. Fig. 4b shows the convergence of the task distance with the number of iterations k in (17); the distance typically converges in 4–5 iterations for these tasks.

Verifying the convergence of coupled transfer We use an iterative algorithm to approximate the optimal couplings between source and target data. Fig. 4a shows the evolution of training and test loss as computed on

samples of the interpolated distribution after 4 iterations of (17). As predicted by Thm. 4 the generalization gap. The training loss increases towards the middle; this is expected because the interpolated distribution is maximally far away from both the source and target data distributions at this point. The convex combination in (17d) keeps computations tractable but could also be a cause for this increase.

We typically require 4–5 iterations of (17) for the task distance to converge; this is shown in Fig. 4b for a few instances. This figure also indicates that computing the transport coupling in (11) independently of the weights and using this coupling to modify the weights, as done in say (Cui et al., 2018), results in a larger distance than if one were to optimize the couplings along with the weights. The coupled transfer finds shorter trajectories for weights and will potentially lead to better accuracies on target tasks in studies like (Cui et al., 2018) because it samples more source data.

Larger capacity results in smaller task distance We next show that using a model with higher capacity results in smaller distances between tasks. We consider a wide residual network (WRN-16-4) of Zagoruyko and Komodakis (2016) and compute distances on subsets of CIFAR-100 in Fig. 5. First note that task distances for coupled transfer in Fig. 5a are consistent with those for fine-tuning in Fig. 5b. Coupled transfer distances in Fig. 5a are much smaller compared to those in Fig. 3a. This is consistent with our argument in Sec. 2.1. Roughly speaking, a high-capacity model can learn a rich set of features, some discriminative and others redundant not relevant to the source task. These redundant features are useful if target task is dissimilar to the source. This experiment also demonstrates that the information-geometric distance computed by coupled transfer can be compared directly across different architectures; this is not so for most methods in the literature to compute distances between tasks. This gives a constructive strategy for selecting architectures for transfer learning.



Figure 5: Fig. 5a shows the task distance using coupled transfer and Fig. 5b show the fine-tuning task distance. The numbers in Fig. 5a can be directly compared to those in Fig. 3a. The larger WRN-16-4 model predicts a smaller task distance for all pairs compared to the smaller convolutional network in Fig. 3a.

5 Related work

Domain-specific methods A rich understanding of task distances has been developed in computer vision, e.g., Zamir et al. (2018) compute pairwise distances when different tasks such as classification, segmentation etc. are performed on the same input data. The goal of this work, and others such as (Cui et al., 2018), is to be able to decide which source data to pre-train to generalize well on a target task. Task distances have also been widely discussed in the multi-task learning (Caruana, 1997) and meta/continual-learning (Liu et al., 2019; Pentina and Lampert, 2014; Hsu et al., 2018). The natural language processing literature also prevents several methods to compute similarity between input data (Mikolov et al., 2013; Pennington et al., 2014).

Most of the above methods are based on evaluating the difficulty of fine-tuning, or computing the similarity in some embedding space. It is difficult to ascertain whether the distances obtained thereby are truly indicative of the difficulty of transfer; fine-tuning hyper-parameters often need to be carefully chosen (Li et al., 2020)

and the embedding space is not unique. For instance, the uncoupled transfer process that modifies the input data distribution will lead to a different estimate of task distance.

Information-theoretic approaches We build upon a line of work that combines generative models and discriminatory classifiers (see (Jaakkola and Haussler, 1999; Perronnin et al., 2010) to name a few) to construct a notion of similarity between input data. Modern variants of this idea include Task2Vec (Achille et al., 2019a) which embeds the task using the diagonal of the FIM and computes distance between tasks using the cosine distance for this embedding. The main hurdle in Task2Vec and similar approaches is to design the architecture for computing FIM: a small model will indicate that tasks are far away. Achille et al. (2019b,c) use the KL divergence between the posterior weight distribution and a prior to quantify the complexity of a task; distance between tasks is defined to be the increase in complexity when the target task is added to the source task. This is an elegant formalism to define task distances but instantiating these ideas for deep networks requires drastic approximations, e.g., a Gaussian posterior on the weight space.

Model complexity Learning theory typically studies out-of-sample performance on a single task. Our goal is to account for the model complexity while defining the task distance. Complexity measures such as VC-dimension (Vapnik, 1998), come with a number of caveats when applied to deep networks because these measures are not reparameterization invariant. We exploited the geometric characterization of the statistical manifold Amari (2016) that leads to invariant quantities such as the Fisher-Rao distance.

Coupled transfer of data and the model A key idea of our work is to observe that the marginal on the input can be transported in addition to the weights of the model. This is motivated from two recent studies. Gao and Chaudhari (2020) develop an algorithm that keeps the classification loss unchanged across transfer. Their method interpolates between the source and target data distribution using a mixture distribution (we use it as a baseline, see Sec. 3.1 and Sec. 4.3). Our work exploits this idea and computes the optimal way to modify both the input distribution and the weights. We use ideas from optimal transportation to compute the transport on input data; see Cui et al. (2018) who also solve an optimal transport problem approximately to estimate task distances. Coupled transport problems on the input data are also solved for unsupervised translation (Alvarez-Melis and Jaakkola, 2018).

6 Discussion

Our work is an attempt to theoretically understand when transfer is easy and when it is not. An often overlooked idea in large-scale transfer learning is that the dataset need not remain fixed to the target task during transfer. We heavily exploit this idea in the present paper and develop an optimization framework to adapt both the input data distribution and the weights from the source to the target. Although a metric is never unique, this gives legitimacy to our task distance. We compute the *shortest* distance in information space, i.e., the manifold of the conditional distributions. It is remarkable that this concept is closely related to the intuitive idea that a good transfer algorithm is one that keeps the generalization gap small during transfer, in particular at the end on the target task.

The most drastic approximation in this paper was to forgo a generative framework for the input distribution. This opens an interesting direction for future work which formulates the distance between tasks simply as the shortest geodesic on the manifold of joint distributions $p_w(x, y)$.

References

Achille, A., Lam, M., Tewari, R., Ravichandran, A., Maji, S., Fowlkes, C. C., Soatto, S., and Perona, P. (2019a). Task2vec: Task embedding for meta-learning. In *Proceedings of the IEEE International Conference on Computer Vision*, pages 6430–6439.

- Achille, A., Mbeng, G., and Soatto, S. (2019b). Dynamics and Reachability of Learning Tasks. *arXiv:1810.02440 [cs, stat]*.
- Achille, A., Paolini, G., Mbeng, G., and Soatto, S. (2019c). The Information Complexity of Learning Tasks, their Structure and their Distance. *arXiv:1904.03292 [cs, math, stat]*.
- Alvarez-Melis, D. and Jaakkola, T. (2018). Gromov-Wasserstein Alignment of Word Embedding Spaces. In *Proceedings of the 2018 Conference on Empirical Methods in Natural Language Processing*, pages 1881–1890, Brussels, Belgium. Association for Computational Linguistics.
- Amari, S.-i. (2016). *Information Geometry and Its Applications*, volume 194 of *Applied Mathematical Sciences*. Springer Japan, Tokyo.
- Bartlett, P. L., Foster, D. J., and Telgarsky, M. J. (2017). Spectrally-normalized margin bounds for neural networks. In *Advances in Neural Information Processing Systems*, pages 6240–6249.
- Bartlett, P. L. and Mendelson, S. (2001). Rademacher and Gaussian Complexities: Risk Bounds and Structural Results. In Goos, G., Hartmanis, J., van Leeuwen, J., Helmbold, D., and Williamson, B., editors, *Computational Learning Theory*, volume 2111, pages 224–240. Springer Berlin Heidelberg, Berlin, Heidelberg.
- Bauer, M., Bruveris, M., and Michor, P. W. (2016). Uniqueness of the Fisher–Rao metric on the space of smooth densities. *Bulletin of the London Mathematical Society*, 48(3):499–506.
- Bauschke, H. H. and Combettes, P. L. (2017). *Convex Analysis and Monotone Operator Theory in Hilbert Spaces*. CMS Books in Mathematics. Springer International Publishing, second edition.
- Carlier, G., Galichon, A., and Santambrogio, F. (2010). From Knothe’s transport to Brenier’s map and a continuation method for optimal transport. *SIAM Journal on Mathematical Analysis*, 41(6):2554–2576.
- Caruana, R. (1997). Multitask learning. *Machine learning*, 28(1):41–75.
- Cui, Y., Song, Y., Sun, C., Howard, A., and Belongie, S. (2018). Large scale fine-grained categorization and domain-specific transfer learning. In *Proceedings of the IEEE Conference on Computer Vision and Pattern Recognition*, pages 4109–4118.
- Cuturi, M. (2013). Sinkhorn distances: Lightspeed computation of optimal transport. In *Advances in Neural Information Processing Systems*, pages 2292–2300.
- Devlin, J., Chang, M.-W., Lee, K., and Toutanova, K. N. (2018). BERT: Pre-training of deep bidirectional transformers for language understanding.
- Dhillon, G. S., Chaudhari, P., Ravichandran, A., and Soatto, S. (2020). A baseline for few-shot image classification. In *Proc. of International Conference of Learning and Representations (ICLR)*.
- Gao, Y. and Chaudhari, P. (2020). A free-energy principle for representation learning. In *Proc. of International Conference of Machine Learning (ICML)*.
- Hsu, K., Levine, S., and Finn, C. (2018). Unsupervised learning via meta-learning. *arXiv preprint arXiv:1810.02334*.
- Hu, J., Lu, J., and Tan, Y.-P. (2015). Deep transfer metric learning. In *Proceedings of the IEEE conference on computer vision and pattern recognition*, pages 325–333.
- Jaakkola, T. and Haussler, D. (1999). Exploiting generative models in discriminative classifiers. In *Advances in Neural Information Processing Systems*, pages 487–493.
- Joulin, A., van der Maaten, L., Jabri, A., and Vasilache, N. (2016). Learning Visual Features from Large Weakly Supervised Data. In Leibe, B., Matas, J., Sebe, N., and Welling, M., editors, *Computer Vision – ECCV 2016*, Lecture Notes in Computer Science, pages 67–84, Cham. Springer International Publishing.
- Kolesnikov, A., Beyer, L., Zhai, X., Puigcerver, J., Yung, J., Gelly, S., and Hounsby, N. (2019). Large scale learning of general visual representations for transfer. *arXiv preprint arXiv:1912.11370*.
- Kornblith, S., Shlens, J., and Le, Q. V. (2019). Do better imagenet models transfer better? In *Proceedings of the IEEE conference on computer vision and pattern recognition*, pages 2661–2671.
- Krizhevsky, A. and Hinton, G. (2009). Learning multiple layers of features from tiny images. Technical report, Citeseer.
- Kunstner, F., Hennig, P., and Balles, L. (2019). Limitations of the empirical Fisher approximation for natural gradient descent. In *Advances in Neural Information Processing Systems*, pages 4156–4167.
- Lee, J., Dabagia, M., Dyer, E., and Rozell, C. (2019). Hierarchical optimal transport for multimodal distribution alignment. In *Advances in Neural Information Processing Systems*, pages 13474–13484.
- Li, H., Chaudhari, P., Yang, H., Lam, M., Ravichandran, A., Bhotika, R., and Soatto, S. (2020). Rethinking the hyper-parameters for fine-tuning. In *Proc. of International Conference of Learning and Representations (ICLR)*.

- Liang, T., Poggio, T., Rakhlin, A., and Stokes, J. (2019). Fisher-rao metric, geometry, and complexity of neural networks. In *The 22nd International Conference on Artificial Intelligence and Statistics*, pages 888–896.
- Liu, C., Lu, T., Sahoo, D., Fang, Y., and Hoi, S. C. (2019). Localized meta-learning: A PAC-Bayes analysis for meta-learning beyond global prior.
- Liu, Z., Luo, P., Qiu, S., Wang, X., and Tang, X. (2016). Deepfashion: Powering robust clothes recognition and retrieval with rich annotations. In *Proceedings of IEEE Conference on Computer Vision and Pattern Recognition (CVPR)*.
- Mahajan, D., Girshick, R., Ramanathan, V., He, K., Paluri, M., Li, Y., Bharambe, A., and van der Maaten, L. (2018). Exploring the limits of weakly supervised pretraining. In *Proceedings of the European Conference on Computer Vision (ECCV)*, pages 181–196.
- McCann, R. J. (1997). A Convexity Principle for Interacting Gases. *Advances in Mathematics*, 128(1):153–179.
- Merkow, J., Lufkin, R., Nguyen, K., Soatto, S., Tu, Z., and Vedaldi, A. (2017). DeepRadiologyNet: Radiologist level pathology detection in CT head images. *arXiv preprint arXiv:1711.09313*.
- Mikolov, T., Chen, K., Corrado, G., and Dean, J. (2013). Efficient estimation of word representations in vector space. *arXiv preprint arXiv:1301.3781*.
- Neyshabur, B., Salakhutdinov, R. R., and Srebro, N. (2015a). Path-sgd: Path-normalized optimization in deep neural networks. In *Advances in Neural Information Processing Systems*, pages 2422–2430.
- Neyshabur, B., Tomioka, R., and Srebro, N. (2015b). Norm-based capacity control in neural networks. In *Conference on Learning Theory*, pages 1376–1401.
- Pennington, J., Socher, R., and Manning, C. D. (2014). Glove: Global vectors for word representation. In *Proceedings of the 2014 Conference on Empirical Methods in Natural Language Processing (EMNLP)*, pages 1532–1543.
- Pentina, A. and Lampert, C. (2014). A PAC-Bayesian bound for lifelong learning. In *International Conference on Machine Learning*, pages 991–999.
- Perronnin, F., Sánchez, J., and Mensink, T. (2010). Improving the fisher kernel for large-scale image classification. In *European Conference on Computer Vision*, pages 143–156. Springer.
- Peyré, G. and Cuturi, M. (2019). Computational Optimal Transport. *arXiv:1803.00567 [stat]*.
- Qi, H., Brown, M., and Lowe, D. G. (2018). Low-shot learning with imprinted weights. In *Proceedings of the IEEE Conference on Computer Vision and Pattern Recognition*, pages 5822–5830.
- Rao, C. (1945). Information and accuracy attainable in the estimation of statistical parameters. Kotz S & Johnson NL (eds.), *Breakthroughs in Statistics Volume I: Foundations and Basic Theory*, 235–248.
- Santambrogio, F. (2015). Optimal transport for applied mathematicians. *Birkhäuser, NY*, 55(58-63):94.
- Shwartz-Ziv, R. and Tishby, N. (2017). Opening the black box of deep neural networks via information. *arXiv preprint arXiv:1703.00810*.
- Snell, J., Swersky, K., and Zemel, R. (2017). Prototypical networks for few-shot learning. In *Advances in Neural Information Processing Systems*, pages 4077–4087.
- Tishby, N., Pereira, F. C., and Bialek, W. (2000). The information bottleneck method. *arXiv preprint physics/0004057*.
- Vapnik, V. (1998). *Statistical Learning Theory*, volume 1. John Wiley & Sons.
- Zagoruyko, S. and Komodakis, N. (2016). Wide residual networks. *arXiv preprint arXiv:1605.07146*.
- Zamir, A. R., Sax, A., Shen, W., Guibas, L. J., Malik, J., and Savarese, S. (2018). Taskonomy: Disentangling task transfer learning. In *Proceedings of the IEEE Conference on Computer Vision and Pattern Recognition*, pages 3712–3722.
- Zhang, H., Cisse, M., Dauphin, Y. N., and Lopez-Paz, D. (2017). Mixup: Beyond empirical risk minimization. *arXiv:1710.09412*.

Appendix A Details of Sec. 2.1

Gao and Chaudhari (2020) modify the Information Bottleneck (IB) Principle (Tishby et al., 2000). The central idea of the IB is to learn a representation z that maximize the mutual information with respect to the targets y and minimize the mutual information with respect to the input x ; this can be written as

$$\min_{e(z|x), c(y|z)} \{R + \gamma C\} \quad (23)$$

where

$$R = \mathbb{E}_{(x,y) \sim p^s} \left[\int dz e(z|x) \log \frac{e(z|x)}{m(z)} \right], \quad \text{and} \quad C = - \mathbb{E}_{(x,y) \sim P} \left[\int dz e(z|x) \log c(y|z) \right].$$

The rate of the encoder R is an upper-bound on the mutual information $I(x, z)$ and C simply denotes the average cross-entropy loss using the representation z to predict y . Since the IB promotes invariance to features in the input that are not necessary to predict the targets accurately, it necessarily entails throwing away redundant information in the data. The authors build upon the observation that this redundant information is potentially useful to learn a new task and introduce a new variational problem

$$F_{p^s}(\lambda, \gamma) = \min_{e(z|x), d(x|z), c(y|z)} \{R + \lambda D + \gamma C\}. \quad (24)$$

The additional term D is the reconstruction error when the representation z is used to decode the back the data x using the decoder $d(x|z)$

$$D = -E_{(x,y) \sim p^s} \left[\int dz e(z|x) \log d(x|z) \right].$$

The idea is that since reconstruction of the data requires learning a lossless representation, including distortion D in problem (24) allows the user to control the amount of information that is thrown away while training on the source task. These authors use the above model to devise a transfer learning algorithm. We instead use this model to provide a heuristic argument of how a low-capacity model is difficult to transfer to the target task.

Appendix B Details of the experimental setup

B.1 Architecture and training.

We show results using an 8-layer convolutional neural network with ReLU nonlinearities, dropout, batch-normalization with a final fully-connected layer along with a larger wide-residual-network (WRN-16-4 architecture of (Zagoruyko and Komodakis, 2016)).

B.2 Transferring between CIFAR-10 and CIFAR-100

We consider four tasks: (i) all vehicles (airplane, automobile, ship, truck) in CIFAR-10, consisting of 20,000 32×32 -sized RGB images; (ii) the remainder, namely six animals in CIFAR-10, consisting of 30,000 32×32 -sized RGB images; (iii) the entire CIFAR-10 dataset and (iv) the entire CIFAR-100 dataset, consisting of 50,000 images and spread across 100 classes.

We pre-train model on source tasks using stochastic gradient descent (SGD) for 60 epochs, with mini-batch size of 20, learning rate schedule is set to 10^{-3} for epochs 0 – 40 and 8×10^{-4} for epochs 40 – 60. When CIFAR-100 is the source dataset, we train for 180 epochs with the learning rate set to 10^{-3} for epochs 0 – 120, and 8×10^{-4} for epochs 120 – 180.

We chose a slightly smaller version of the source and target datasets to compute the distance, each of them have 19,200 images. The class distribution on all source and target classes is balanced. We did this to reduce the size of the coupling matrix Γ in (17a). The coupling matrix connecting inputs in the source and target datasets is $\Gamma \in \mathbb{R}^{19200 \times 19200}$ which is still quite large to be tractable during optimization. We therefore use a block diagonal approximation of the coupling matrix; 640 blocks are constructed each of size 30×30 and all other entries in the coupling matrix are set to zero at the beginning of each iteration in (17a) after computing the dense coupling matrix using the linear program. This effectively entails that the set of couplings over which we compute the transport is not the full convex polytope in (10) but rather a subset of it. We sample a mini-batch of 20 images from the interpolated distribution corresponding to this block-diagonal coupling matrix for each weight update of (17c). We run 40 epochs, i.e., with $19200/20 = 960$ weight updates per epoch for computing the weight trajectory at *each iteration* k in (17). The learning rate is fixed to 8×10^{-4} in the transfer learning phase.

B.3 Transferring among subsets of CIFAR-100

The same 8-layer convolutional network is used to show results for transfer between subsets of CIFAR-10 and CIFAR-100. CIFAR-10 is split into the two tasks animals and vehicle again. We construct five tasks (herbivores, carnivores, vehicles-1, vehicles-2 and flowers) that are subsets of the CIFAR-100 dataset. Each of these tasks consists of 5 sub-classes.

We train the model on the source task using SGD for 400 epochs with a mini-batch size of 20. Learning rate is set to 10^{-3} for epochs 0 – 240, and to 8×10^{-4} for epochs 240 – 400.

Tasks that are subsets of CIFAR-100 in the experiments in this section have few samples (2500 each) so we select 2400 images from source and target datasets respectively; we could have chosen a larger source dataset when transferring from CIFAR-10 animals or vehicles but we did not so for sake of simplicity. The number 2400 was chosen to make the block diagonal approximation of the coupling matrix have 120×120 entries in each block; this was constrained by the GPU memory. The coupling matrix Γ therefore has 2400×2400 entries with 20 blocks on the diagonal.

Again, we use a mini-batch size of 20 for 240 epochs ($2400/20 = 120$ weight updates per epoch) during the transfer from the source dataset to the target dataset. The learning rate is fixed to 8×10^{-4} in the transfer learning phase.

B.4 Training setup for wide residual network

We pre-train WRN-16-4 on source tasks using SGD for 400 epochs with a mini-batch size of 20. Learning rate is 10^{-1} for epochs 0 – 120, 2×10^{-2} for epochs 120 – 240, 4×10^{-3} for epochs 240–320, and 8×10^{-4} for epochs 320 – 400. Other experimental details are the same as those in Sec. B.3.

Appendix C Additional experiments on the Deep Fashion dataset

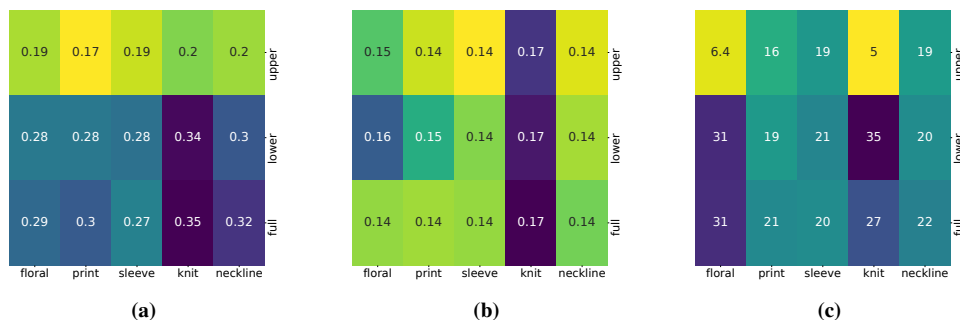


Figure 6: Fig. 6a shows distances (numbers in the cell) among sub-tasks in DeepFashion computed using our coupled transfer process, Fig. 6b shows distances estimated using Task2Vec while Fig. 6c shows distances estimated using fine-tuning. Numerical values of the distances in this figure are not comparable with each other. Coupled transfer, Task2Vec and fine-tuning all agree with that transferring to knit is relatively hard. Transferring from upper-cloth to knit is easy via fine-tuning and coupled transfer correctly estimates this distance to be small; the distance estimated by Task2Vec is much larger in comparison.

For the Deep Fashion dataset (Liu et al., 2016), we consider three binary category classification tasks (upper clothes, lower clothes, and full clothes) and five binary attribute classification tasks (floral, print, sleeve, knit, and neckline). We show results in Fig. 6 using 3×5 distance matrices where numbers in each cell indicate the distance between the source task (row) and the target task (column). We show results using a wide-residual-network (WRN-16-4, (Zagoruyko and Komodakis, 2016)).

The model is trained using SGD for 400 epochs with a mini-batch size 20. Learning rate is 10^{-1} for epochs 0 – 120, 2×10^{-2} for epochs 120 – 240, 4×10^{-3} for epochs 240–320, and 8×10^{-4} for epochs 320 – 400.

We sample 14,000 images from the source and target datasets to compute distances. A mini-batch size of 20 is used during transfer and we run (17c) for 60 epochs (14000/20 = 700 weight updates per epoch).

Appendix D Proof of Thm. 4

Given a trajectory of the weights $\{w_\tau\}_{\tau \in [0,1]}$ and a sequence $0 \leq \tau_1 < \tau_2 < \dots < \tau_K \leq 1$, then for all $\epsilon > \frac{2}{K} \sum_{k=1}^K \mathcal{R}_N(\|w_{t_k}\|_{\text{fr}})$, the probability that

$$\frac{1}{K} \sum_{k=1}^K \left(\mathbb{E}_{(x,y) \sim p_{\tau_k}} [\ell(w_{\tau_k}, x, y)] - \frac{1}{N} \sum_{(x,y) \sim \hat{p}_{\tau_k}} \ell(w_{\tau_k}, x, y) \right)$$

is greater than ϵ is upper bounded by

$$\exp \left\{ -\frac{2K}{M^2} \left(\epsilon - \frac{2}{K} \sum_{k=1}^K \mathcal{R}_N(\|w_{t_k}\|_{\text{fr}}) \right)^2 \right\}. \quad (25)$$

Proof. For each moment τ_k , by taking supremum

$$\mathbb{E}_{(x,y) \sim p_{\tau_k}} \ell(w_{\tau_k}, x, y) - \frac{1}{N} \sum_{(x,y) \sim \hat{p}_{\tau_k}} \ell(w_{\tau_k}, x, y) \leq \sup_{\|w\|_f \leq \|w_{\tau_k}\|_f} \left(\mathbb{E}_{(x,y) \sim p_{\tau_k}} \ell(w, x, y) - \frac{1}{N} \sum_{(x,y) \sim \hat{p}_{\tau_k}} \ell(w, x, y) \right), \quad (26)$$

where $\|\cdot\|_f$ denotes Fisher-Rao norm. The right hand side of inequality(26) is a random variable that depends on the drawn sampling set \hat{p}_{τ_k} . Denoting

$$\phi(\hat{p}_{\tau_k}) := \sup_{\|w\|_f \leq \|w_{\tau_k}\|_f} \left(\mathbb{E}_{(x,y) \sim p_{\tau_k}} \ell(w, x, y) - \frac{1}{N} \sum_{(x,y) \sim \hat{p}_{\tau_k}} \ell(w, x, y) \right), \quad (27)$$

We would like to bound the expectation of $\phi(\hat{p}_{\tau_k})$ in terms of the Rademacher complexity. In order to do this, we introduce a ‘‘ghost sample’’ with size N , \hat{p}'_{τ_k} , independently drawn identically from $p_{\tau_k}(x, y)$, we rewrite the expectations

$$\begin{aligned} \mathbb{E}_{\hat{p}_{\tau_k}} \phi(\hat{p}_{\tau_k}) &= \mathbb{E}_{\hat{p}_{\tau_k}} \left[\sup_{\|w\|_f \leq \|w_{\tau_k}\|_f} \left(\mathbb{E}_{(x,y) \sim p_{\tau_k}} \ell(w, x, y) - \frac{1}{N} \sum_{(x,y) \sim \hat{p}_{\tau_k}} \ell(w, x, y) \right) \right] \\ &= \mathbb{E}_{\hat{p}_{\tau_k}} \left[\sup_{\|w\|_f \leq \|w_{\tau_k}\|_f} \mathbb{E}_{\hat{p}'_{\tau_k}} \left(\frac{1}{N} \sum_{(x,y) \sim \hat{p}'_{\tau_k}} \ell(w, x, y) - \frac{1}{N} \sum_{(x,y) \sim \hat{p}_{\tau_k}} \ell(w, x, y) \right) \right] \\ &\leq \mathbb{E}_{\hat{p}_{\tau_k}, \hat{p}'_{\tau_k}, \sigma} \left[\sup_{\|w\|_f \leq \|w_{\tau_k}\|_f} \frac{1}{N} \left(\sum_{(x,y) \sim \hat{p}_{\tau_k}} \sigma^i (\ell(w, x, y) - \ell(w, x, y)) \right) \right] \\ &\leq \mathbb{E}_{\hat{p}_{\tau_k}, \sigma} \left[\sup_{\|w\|_f \leq \|w_{\tau_k}\|_f} \frac{1}{N} \sum_{(x,y) \sim \hat{p}_{\tau_k}} \sigma^i \ell(w, x, y) \right] + \mathbb{E}_{\hat{p}_{\tau_k}, \sigma} \left[\sup_{\|w\|_f \leq \|w_{\tau_k}\|_f} \frac{1}{N} \sum_{(x,y) \sim \hat{p}_{\tau_k}} \sigma^i \ell(w, x, y) \right] \\ &= 2\mathcal{R}_N(\|w_{\tau_k}\|_f), \end{aligned}$$

where $\sigma = (\sigma^1, \sigma^2, \dots, \sigma^N)$ are independent random variables drawn from the Rademacher distribution, the last equality is followed by the definition of Rademacher Complexity within $\|w_{\tau_k}\|_f$ -ball in the Fisher-Rao norm. By the Hoeffding's lemma, for $\lambda > 0$

$$\begin{aligned} \mathbb{E}_{\hat{p}_{\tau_k}} \exp \left\{ \lambda \left(\mathbb{E}_{(x,y) \sim p_{\tau_k}} \ell(w_{\tau_k}, x, y) - \frac{1}{N} \sum_{(x,y) \sim \hat{p}_{\tau_k}} \ell(w_{\tau_k}, x, y) \right) \right\} &= \mathbb{E}_{\hat{p}_{\tau_k}} e^{\lambda \phi(\hat{p}_{\tau_k})} \\ &\leq e^{\lambda \mathbb{E}_{\hat{p}_{\tau_k}} \phi(\hat{p}_{\tau_k}) + \frac{\lambda^2 M^2}{8}} \\ &\leq e^{2\lambda \mathcal{R}_N(\|w_{\tau_k}\|_f) + \frac{\lambda^2 M^2}{8}}. \end{aligned} \quad (28)$$

For each moment τ_k , we have inequality(28), which implies

$$\begin{aligned} &\mathbb{E}_{\hat{p}_{\tau_k}: 1 \leq k \leq K} \exp \left\{ \lambda \sum_{k=1}^K \left(\mathbb{E}_{(x,y) \sim p_{\tau_k}} \ell(w_{\tau_k}, x, y) - \frac{1}{N} \sum_{(x,y) \sim \hat{p}_{\tau_k}} \ell(w_{\tau_k}, x, y) \right) \right\} \\ &= \prod_{k=1}^K \mathbb{E}_{\hat{p}_{\tau_k}} \exp \left\{ \lambda \left(\mathbb{E}_{(x,y) \sim p_{\tau_k}} \ell(w_{\tau_k}, x, y) - \frac{1}{N} \sum_{(x,y) \sim \hat{p}_{\tau_k}} \ell(w_{\tau_k}, x, y) \right) \right\} \\ &\leq \exp \left\{ \sum_{k=1}^K \left[2\lambda \mathcal{R}_N(\|w_{\tau_k}\|_f) + \frac{\lambda^2 M^2}{8} \right] \right\}. \end{aligned}$$

Finally for all $K\epsilon > 2 \sum_{k=1}^K \mathcal{R}_N(\|w_{t_k}\|_{fr})$, by Markov inequality

$$\begin{aligned} Pr \left\{ \sum_{k=1}^K \left(\mathbb{E}_{(x,y) \sim p_{\tau_k}} \ell(w_{\tau_k}, x, y) - \frac{1}{N} \sum_{(x,y) \sim \hat{p}_{\tau_k}} \ell(w_{\tau_k}, x, y) \right) > K\epsilon \right\} \\ \leq \exp \left\{ -\lambda K\epsilon + \sum_{k=1}^K \left[2\lambda \mathcal{R}_N(\|w_{\tau_k}\|_f) + \frac{\lambda^2 M^2}{8} \right] \right\} \end{aligned} \quad (29)$$

Put $\lambda = \frac{4K(\epsilon - \frac{2}{K} \sum_{k=1}^K \mathcal{R}_N(\|w_{t_k}\|_{fr}))}{M^2}$ in right hand side of inequality(29), then we finish the proof. \square

Appendix E A refined result on the connection between the Fisher-Rao distance on the manifold and generalization error on the interpolating distribution

The upper bound in (29) above states that we should minimize the Rademacher complexity of the hypothesis space in order to ensure that the weight trajectory has a small generalization gap at all time instants. For linear models, as discussed in the main paper, the Rademacher complexity can be related to the Fisher-Rao norm $\langle w, gw \rangle$. The Fisher-Rao distance on the manifold, namely

$$\int_0^1 \mathbb{E}_{x \sim p_\tau(x)} \left[\sqrt{2\text{KL}(p_{w_\tau}(\cdot|x), p_{w_{\tau+d\tau}}(\cdot|x))} \right] d\tau = \int_0^1 \mathbb{E}_{x \sim p_\tau(x)} \sqrt{\langle \dot{w}_\tau, g(w_\tau) \dot{w}_\tau \rangle} d\tau$$

is only a lower bound on the integral of the Fisher-Rao norm along the weight trajectory. We therefore make some additional assumptions in this section to draw out a crisp link between the Fisher-Rao *distance* and generalization gap along the trajectory.

Let $\ell(w; x, y) := -\log p_w(y|x)$ be the cross-entropy loss on sample (x, y) . We assume that at each moment $\tau \in [0, 1]$, our model $p_{w_\tau}(y|x)$ predicts on the interpolating distribution $p_\tau(y|x)$ well, that is

$$p_{w_\tau}(y|x) \approx p_\tau(y|x)$$

for all input x ; this is a reasonable assumption and corresponds to taking a large number of mini-batch updates in (17c). We approximate the FIM using the empirical FIM, i.e., we approximate the distribution $p_\tau(y|x)$ as a Dirac-delta distribution on the interpolated labels $y_\tau(x)$. Observe that

$$\begin{aligned} \langle \dot{w}_\tau, g(w_\tau) \dot{w}_\tau \rangle &= \left\langle \dot{w}_\tau, \mathbb{E}_{y|x \sim p_{w_\tau}} \partial_w \ell_{w_\tau}(y|x) \partial_w \ell_{w_\tau}(y|x)^\top \dot{w}_\tau \right\rangle \\ &\approx \langle \dot{w}_\tau, \partial_w \ell(w_\tau; x, y_\tau(x)) \partial_w \ell(w_\tau; x, y_\tau(x))^\top \dot{w}_\tau \rangle \\ &= \left| \frac{\ell(w_{\tau+d\tau}; x, y_\tau(x)) - \ell(w_\tau; x, y_\tau(x))}{d\tau} \right|^2 \\ &= \left| \frac{\Delta \ell(w_\tau)}{d\tau} \right|^2, \end{aligned} \quad (30)$$

where we use the shorthand

$$\Delta \ell(w_\tau) := \ell(w_{\tau+d\tau}; x, y_\tau(x)) - \ell(w_\tau; x, y_\tau(x)),$$

and plug (30) in the integration in (1)

$$\begin{aligned} \int_0^1 \mathbb{E}_{x \sim p_\tau(x)} \left[\sqrt{2\text{KL}(p_{w_\tau}(\cdot|x), p_{w_{\tau+d\tau}}(\cdot|x))} \right] d\tau &= \int_0^1 \mathbb{E}_{x \sim p_\tau(x)} \sqrt{\langle \dot{w}_\tau, g(w_\tau) \dot{w}_\tau \rangle} d\tau \\ &\approx \int_0^1 \mathbb{E}_{x \sim p_\tau(x)} [|\Delta \ell(w_\tau)|] d\tau. \end{aligned} \quad (31)$$

On the other hand, for moment τ let $\Omega_\tau \ni w_\tau$ be a neighborhood of w_τ in weights space, Rademacher complexity of the class of loss function is upper bounded as following

$$\begin{aligned} \mathcal{R}_N(\Omega_\tau) &= \mathbb{E}_{\hat{p} \sim p_\tau} \mathbb{E}_\sigma \left[\sup_{w \in \Omega_\tau} \frac{1}{N} \sum_{i=1}^N \epsilon^i \ell(w; x^i, y^i) \right] \\ &= \mathbb{E}_{\hat{p} \sim p_\tau} \mathbb{E}_\sigma \left[\sup_{w \in \Omega_\tau} \frac{1}{N} \sum_{i=1}^N \epsilon^i \ell(w_\tau; x^i, y^i) + \epsilon^i (\ell(w; x^i, y^i) - \ell(w_\tau; x^i, y^i)) \right] \\ &\leq \mathbb{E}_{\hat{p} \sim p_\tau} \mathbb{E}_\sigma \left[\frac{1}{N} \sum_{i=1}^N \epsilon^i \ell(w_\tau; x^i, y^i) + \sup_{w \in \Omega_\tau} \frac{1}{N} \sum_{i=1}^N |\ell(w; x^i, y^i) - \ell(w_\tau; x^i, y^i)| \right], \\ &= \mathbb{E}_{\hat{p} \sim p_\tau} \left[0 + \sup_{w \in \Omega_\tau} \frac{1}{N} \sum_{i=1}^N |\ell(w; x^i, y^i) - \ell(w_\tau; x^i, y^i)| \right] \\ &\rightarrow \sup_{w \in \Omega_\tau} \mathbb{E}_{x \sim p_\tau} |\ell(w; x, y_\tau(x)) - \ell(w_\tau; x, y_\tau(x))| \end{aligned} \quad (32)$$

as N goes to infinity. Let

$$\Omega_\tau := \{w \mid \mathbb{E}_{x \sim p_\tau} |\ell(w; x, y_\tau(x)) - \ell(w_\tau; x, y_\tau(x))| \leq \mathbb{E}_{x \sim p_\tau} |\ell(w_{\tau+d\tau}; x, y_\tau(x)) - \ell(w_\tau; x, y_\tau(x))|\}, \quad (33)$$

be the neighborhood of w_τ within which the loss function changes less than $|\Delta \ell(w_\tau)|$. Compare this with (31), the Rademacher complexity of Ω_τ is exactly upper bounded by integration increments appearing in the expression for the Fisher-Rao distance. If we substitute $\|w_\tau\|_{\text{fr}}$ in Thm. 4 with this modified Ω_τ , we have the following theorem.

Theorem 6. Given a trajectory of the weights $\{w_\tau\}_{\tau \in [0,1]}$ and a sequence $0 = \tau_0 \leq \tau_1 < \tau_2 < \dots < \tau_K \leq 1$, for all $\epsilon > 2 \sum_{k=1}^K (\tau_k - \tau_{k-1}) \mathbb{E}_{x \sim p_\tau} |\Delta \ell(w_{\tau_{k-1}})|$, the probability that

$$\frac{1}{K} \sum_{k=1}^K \left(\mathbb{E}_{(x,y) \sim p_{\tau_k}} [\ell(w_{\tau_k}, x, y)] - \frac{1}{N} \sum_{(x,y) \sim \hat{p}_{\tau_k}} \ell(w_{\tau_k}, x, y) \right)$$

is greater than ϵ is upper bounded by

$$\exp \left\{ -\frac{2K}{M^2} \left(\epsilon - 2 \sum_{k=1}^K (\tau_k - \tau_{k-1}) \mathbb{E}_{x \sim p_{\tau_k}} [|\Delta \ell(w_{\tau_{k-1}})|] \right) \right\}. \quad (34)$$

Proof. The proof is same as in Thm. 4 except for substituting $\mathcal{R}_N(\|w_{\tau_k}\|_{\text{fr}})$ with $\mathcal{R}_N(\Omega_{\tau_k})$ and using upper bounds (32), and

$$\begin{aligned} \Omega_{\tau_k} &= \{w \mid \mathbb{E}_{x \sim p_{\tau_k}} |\ell(w; x, y_{\tau_k}(x)) - \ell(w_{\tau_k}; x, y_{\tau_k}(x))|\} \\ &\leq K(\tau_k - \tau_{k-1}) \mathbb{E}_{x \sim p_{\tau_k}} |\ell(w_{\tau_k}; x, y_{\tau_k}(x)) - \ell(w_{\tau_{k-1}}; x, y_{\tau_k}(x))|. \end{aligned} \quad (35)$$

□

We can now relate the Fisher-Rao distance (1) and the generalization bound in Thm. 6. For instance, if $|\frac{d}{d\tau} \ell(w_\tau; x, y_\tau(x))|$ is Riemann integrable over τ , then as K goes to infinity, there exists a sequence $0 = \tau_0 \leq \tau_1 < \tau_2 < \dots < \tau_K \leq 1$ such that

$$\begin{aligned} \sum_{k=1}^K (\tau_k - \tau_{k-1}) \mathbb{E}_{x \sim p_{\tau_k}} |\ell(w_{\tau_k}; x, y_{\tau_k}(x)) - \ell(w_{\tau_{k-1}}; x, y_{\tau_k}(x))| &\longrightarrow \int_0^1 \mathbb{E}_{x \sim p_\tau(x)} |\ell(w_{\tau+d\tau}; x, y_\tau(x)) - \ell(w_\tau; x, y_\tau(x))| \\ &\approx \int_0^1 \mathbb{E}_{x \sim p_\tau(x)} \left[\sqrt{2\text{KL}(p_{w_\tau}(\cdot|x), p_{w_{\tau+d\tau}}(\cdot|x))} \right] d\tau. \end{aligned} \quad (36)$$

This shows that computing the Fisher-Rao distance between two points on the statistical manifold results in a weight trajectory that minimizes the the generalization gap of weights trained on the interpolated distribution along the trajectory. In other words, one may either think of our coupled transfer process as computing the Fisher-Rao distance or as finding a weight trajectory that connects weights with a small generalization gap.